This article has been accepted for publication in a future issue of this journal, but has not been fully edited. Content may change prior to final publication. Citation information: DOI 10.1109/LPT.2020.3014695, IEEE Photonics Technology Letters

High Enhancement Strain Sensor based on Vernier Effect using 2-Fiber Loop Mirrors

Paulo Robalinho, André D. Gomes and Orlando Frazão

***Abstract*— In this letter, a strain sensor with high sensitivity enhancement using a special case of Vernier effect is presented. The sensor configuration is composed of two-fiber loop mirrors in series with opposite strain responses when individually characterized. Thus, the enhanced Vernier effect is explored, which is the most sensitive of three possible cases Vernier effect. Here, the Vernier response depends on the difference between the sensitivities of each Hi-Bi optical fiber. In addition to this, the fundamental and the first harmonic were also explored. The results obtained are a strain sensitivity of (13.3 ± 0.3) pm/με for the carrier, (80.0 ± 0.3) pm/με for the Vernier envelope of the fundamental case and (120 ± 1) pm/με for the Vernier envelope of the first harmonic. The first harmonic could achieve a magnification factor of 8. Considering that the optical interrogation system allows a minimum resolution of 0.02 nm, the minimum measurement step achievable is 0.2 με. This work proves the possibility of applying the concept of enhanced Vernier effect to fiber loop mirrors, obtaining higher sensitivity than a standard fiber loop mirror alone. Besides, the sensitivity can be increased through the usage of harmonics of the Vernier effect. Moreover, the use of large interferometers allows a better discretization of the envelope, which implies a greater ease of analysis.**

***Index Terms*—Fiber Loop Mirror, Optical Fiber Sensor, Strain Sensor, Vernier Effect.**

I. Introduction

THE impact of optical systems has been growing in the field of sensors. This phenomenon was made possible by the creation of fiber optics at the beginning of the 20th century. However, its first major demonstration occurred in the 1960s [1]. Fiber optics allowed the transmission of signals over long distances with low attenuations [2], in addition to being easily manufactured and insensitive to electromagnetic fields. These features are of great importance for optical sensors and for optical systems.

In the 1980s, high-birefringent (Hi-Bi) optical fibers have appeared [3]. Hi-Bi fibers can maintain a linear polarization along the beam propagation. In addition, they are composed of two axes (fast and slow axes) with different refractive indices, resultant from the design of the fiber. Some examples of Hi-Bi fibers are e-core [4], D-type [5], Panda [6], Bow-tie [7], and internal elliptical cladding (IEC) [8]. Recently, a photonic crystal fiber (PCF) with birefringence was demonstrated [9]. Due to the property of birefringence, interferometers with Hi-Bi fibers can be easily fabricated. One of them is the fiber loop mirror (FLM) [10]. The FLM allows the creation of two identical waves that travel through the optical system in opposite directions. Both, the division of the input beam into two waves and their recombination, is ensured by an optical fiber coupler. The use of a polarization controller allows to control and adjust the polarization state of the propagating light into the orthogonal polarization of the Hi-Bi optical fiber. This way, two distinct optical paths are created. These two waves interfere with each other at the output, once they have reached the coupler, due to the difference of phase accumulated during the propagation in the Hi-Bi fiber. This type of configuration has been widely used for sensing applications, such as temperature [11], strain [12], pressure [13], and torsion [14].

In 2011, the first fiber sensor based on the Vernier effect was demonstrated [15]. This effect consists of the beating resulting from overlap between two interferometric signals. The output signal is composed of a carrier and an envelope modulation, being the last the main focus of the investigations. The Vernier effect [16] has been increasingly applied throughout this decade due to the ease of enhancing the sensitivity of fiber sensors. Moreover, the Vernier effect makes the implementation of old configurations viable again. However, the application of the Vernier effect can be complex, namely in the practical implementation, as well as in the analysis of the experimental data.

Currently, a strain sensor based on two Fabry–Perot interferometers (FPIs) in reflection, made from capillary tubes in a parallel configuration, could obtain a sensitivity of 93.4 pm/με from 0 – 600 με [17]. Two FPIs in reflection and cascaded achieved a sensitivity of 28.11 pm/με between 0 – 1600 με [18]. A hollow microsphere coupled to a capillary (two FPIs) reached a sensitivity of 146.3 pm/με in the range of 0 – 600 με [19]. Moreover, a Sagnac interferometer coupled to a fiber modal interferometer (FMI) was demonstrated to achieve a sensitivity of 65.7 pm/με from 0 - 300 με [20]. An FLM with two misaligned panda fibers with a sensitivity of 58 pm/με in a range of 0 – 1000 με was also reported [21].

André Gomes is funded by FCT (SFRH/BD/129428/2017).

P. Robalinho (e-mail: paulo.robalinho@inesctec.pt), A. D. Gomes (email: adgomes@inesctec.pt) and O. Frazão (e-mail: ofrazao@inesctec.pt) are with INESC TEC, 4169-007 Porto, Portugal.

A. D. Gomes is also with the Leibniz Institute of Photonic Technology (IPHT), Albert Einstein Str. 9; 07745 Jena, Germany.

This article has been accepted for publication in a future issue of this journal, but has not been fully edited. Content may change prior to final publication. Citation information: DOI 10.1109/LPT.2020.3014695, IEEE Photonics Technology Letters

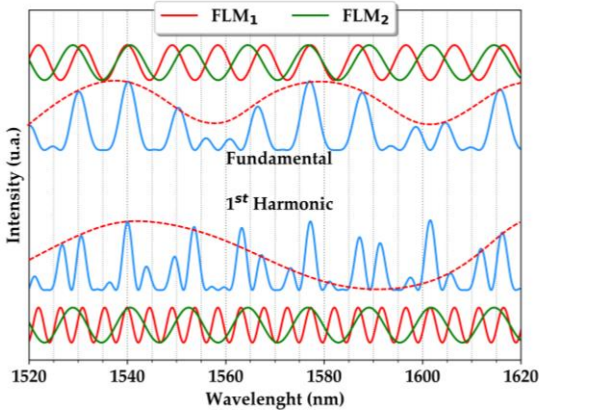

Fig. 1. Vernier effect simulation: two fiber loop mirrors spectrum (FLM), Fundamental and 1st Harmonic. The values used are the experimental ones.

The aim of this work is to explore a strain sensor using the enhanced Vernier effect in order to obtain a high sensitivity. The use of two FLMs in series made of distinct Hi-Bi fibers with opposite strain sensitivities is explored. In such situation, the strain sensitivity enhancement provided by the optical Vernier effect depends on the difference between the FMLs sensitivities. Since the FLMs have opposite strain sensitivities, their contribution to the Vernier effect response will add up, providing additional sensitivity enhancement. Due to the possibility of using large fiber lengths, the fundamental and the first harmonic of the Vernier effect can be easily introduced, being a novelty in FLM configurations.

II. Theoretical Consideration

A fiber loop mirror is composed of a polarization controller, a fiber coupler, and a Hi-Bi optical fiber [22]. The mode of operation starts by dividing the input beam into two beams. The polarization controller allows the polarization of these two beams to be perpendicular to each other when passing through the Hi-Bi optical fiber. Hence, they are subjected to different refractive indices, and thus to two distinct optical paths. Then, these beams are recombined by means of the coupler, resulting in an interference. This system is a non-balanced Mach-Zehnder interferometer where the phase difference ($\Delta\phi$) between the two optical paths is $2\pi\beta L/\lambda$, where β is the birefringence, λ is the wavelength, and L is the Hi-Bi fiber length [23]. The free spectral range (FSR), $\Delta\lambda$, is defined as $\lambda^2/\beta L$ [24]. For an FLM, the output intensity is given by:

$$I_{out}^{FLM}(\lambda) \propto A cos^2\left(\frac{\pi}{\lambda}\beta L\right). \quad (1)$$

The output intensity, normalized to the input, is obtained through [17]:

$$I(\lambda) = \left|\frac{E_{out}(\lambda)}{E_{in}(\lambda)}\right|^2 = \left|\frac{E_{out}(\lambda).E_{out}^*(\lambda)}{E_{in}^2(\lambda)}\right|, \quad (2)$$

where $E_{out}^*(\lambda)$ is the complex conjugate of the output electric field, $E_{out}(\lambda)$. The interference between the two optical paths in the FLM results in a cosinusoidal spectrum, as seen in Fig. 1.

The fundamental Vernier effect can be introduced by adding

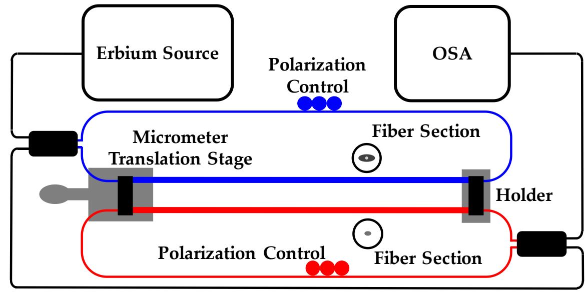

Fig. 2. Setup configuration using two fiber loop mirrors in serie.

two FLMs in series and with similar optical path lengths. The electrical output field of the structure consists now in the product of the two FLMs electrical fields. The normalized output intensity of the Vernier spectrum can then be obtained through eq. 2. For such case, the output intensity is proportional to the sum (carrier) and difference (envelope) between the frequencies of the two FLMs, which can be written as:

$$I \propto \frac{1}{2}cos\left(\frac{2\pi}{\lambda}[\beta_1 L_1 - \beta_2 L_2]\right) + \frac{1}{2}cos\left(\frac{2\pi}{\lambda}[\beta_1 L_1 + \beta_2 L_2]\right) + 2\,cos\left(\frac{\pi}{\lambda}[\beta_1 L_1 - \beta_2 L_2]\right)\cdot cos\left(\frac{\pi}{\lambda}[\beta_1 L_1 + \beta_2 L_2]\right), \quad (3)$$

where the indices 1 and 2 correspond to the first and the second FLM, respectively. As seen from Fig. 1, the maxima of the Vernier envelope occur at the wavelengths where the two interferometers are in phase. Hence, when the spectrum of each interferometer shifts, the Vernier envelope will also shift.

The first harmonic of the Vernier effect can also be introduced to this configuration. Typically, it is obtained by increasing the optical path of one of the interferometers [17], which for this case corresponds to $\beta_2 L_2 \to \beta_2 L_2 + \beta_1 L_1$. The spectrum for the first harmonic is also depicted in Fig. 1.

To obtain an equation to predict the evolution of the spectrum with the variation applied strain, the FSR can be rewritten so that $\Delta\lambda = \lambda^2/(\beta L + B\,Sens\,\varepsilon)$, where ε is the applied strain and B is a constant. Therefore, equation 4 is now expressed as:

$$I \propto \frac{1}{2}cos\left(\frac{2\pi}{\lambda}[\beta_1 L_1 - \beta_2 L_2 + \delta_{env}]\right) + \frac{1}{2}cos\left(\frac{2\pi}{\lambda}[\beta_1 L_1 + \beta_2 L_2 + \delta_{carr}]\right) + 2\,cos\left(\frac{\pi}{\lambda}[\beta_1 L_1 - \beta_2 L_2 + \delta_{env}]\right)\cdot cos\left(\frac{\pi}{\lambda}[\beta_1 L_1 + \beta_2 L_2 + \delta_{carr}]\right), \quad (4)$$

where $\delta_{env} = B(Sens_1 - Sens_2)\varepsilon$ and $\delta_{carr} = B(Sens_1 + Sens_2)\varepsilon$. There are three types of Vernier effect [24]: traditional, reduced, and enhanced. In the traditional Vernier effect one of the interferometers is fixed, while the other changes with the physical parameter being measured. In the reduced Vernier effect both interferometers act as sensors and have the same sensitivity signal (both positive or both negative). Hence, their interferometric responses cancel each other, leading to a lower Vernier sensitivity compared to the traditional case. In the enhanced Vernier effect, as explored in this work, the responses of the interferometers have opposite directions. Hence, their contribution to the Vernier effect adds, resulting in a higher sensitivity compared to the traditional case.

Another important concept is the magnification factor (*M*-factor). In the literature, the *M*-factor allows to compare the

This article has been accepted for publication in a future issue of this journal, but has not been fully edited. Content may change prior to final publication. Citation information: DOI 10.1109/LPT.2020.3014695, IEEE Photonics Technology Letters

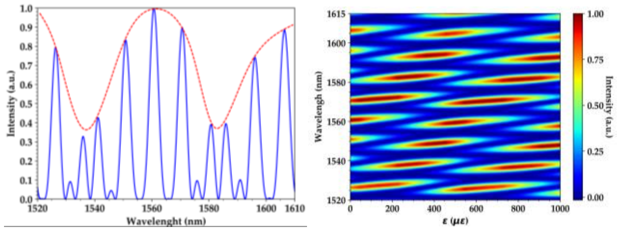

(a) (b)

Fig. 3. Output signal for the fundamental Vernier effect: (a) initial optical spectrum (the upper Vernier envelope is marked with a dashed line); (b) 2D representation of the spectral shift when strain is applied.

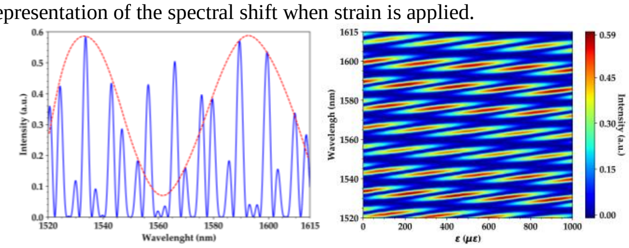

(a) (b)

Fig. 4. Output signal for the 1st harmonic of the Vernier effect: (a) initial optical spectrum (the upper Vernier envelope is marked with a dashed line); (b) 2D representation of the spectral shift when strain is applied.

sensitivity of the envelope with the sensitivity of the sensing interferometer. The *M*-factor can be defined as [25]:

$$M = \text{sens}_{env}/\text{sens}_1 \tag{5}$$

However, such definition does not allow a correct evaluation of the Vernier effect when both interferometers act as sensors. Thus, two new descriptions of the *M*-factor are introduced:

$$M_{\text{FSR}} = \Delta\lambda_{env}/\Delta\lambda_{carr} \tag{6}$$

$$M_{\text{Sens}} = \text{Sens}_{env}/\text{Sens}_{carr} \tag{7}$$

To determine the efficiency of the Vernier effect considering the three possible cases, a new parameter can be defined:

$$M_{\text{Vernier}} = M_{\text{Sens}}/M_{\text{FSR}} \tag{8}$$

The M_{FSR} is independent of each case, since it only depends on the frequency of the interferometers. However, M_{Sens} depends on the sensitivity of the envelope, which is distinct for each possible case. In the traditional case $M_{\text{Sens}} = M_{\text{FSR}}$, as demonstrated in [17]. Therefore, M_{Vernier} is equal to 1. In the reduced case $M_{\text{Sens}} < M_{\text{FSR}}$, since the responses of the two interferometers counter each other, reducing the sensitivity of the Vernier effect. Hence, it implies that $M_{\text{Vernier}} < 1$. For the enhanced case $M_{\text{Sens}} > M_{\text{FSR}}$, since the responses of the two interferometers add up, increasing the sensitivity of the Vernier effect. Therefore, $M_{\text{Vernier}} > 1$.

III. Setup Configuration

The setup shown in Fig. 2 was used to characterize the sensing configuration with high enhancement using the Vernier effect. The setup consists of two-fiber loop mirrors in series. Each one includes a 3 dB (2×2) optical coupler with low insertion losses, an optical fiber polarization controller, and a Hi-Bi optical fiber section. The first fiber loop mirror has an

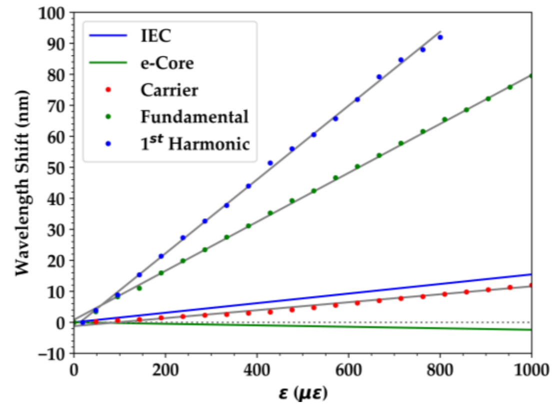

Fig. 5. Wavelength shift for Carrier and Envelopes.

internal elliptical cladding (IEC) fiber section with a $\beta = 5.1 \times 10^{-4}$, while the second fiber loop mirror has an e-core fiber section with a $\beta = 3.85 \times 10^{-4}$. In addition, an erbium broadband source centered at 1550 nm and with a bandwidth of 100 nm was connected to the input, while the output was monitored using an optical spectrum analyzer (OSA) ("YOKOGAWA AQ5370C") with a resolution of 0.02 nm. Standard fiber (SMF28) was used to connect the different subsystems. The splices between the specialty fibers and the SMF28 were made using a conventional splice machine ("Sumitomo Electric Type-72C", Osaka, Japan). The fundamental Vernier effect (see Fig. 3) was introduced using an IEC fiber section with a length of (0.521 ± 0.001) m, generating an FLM spectrum with a FSR of 9 nm, and an e-core fiber section with a length of (0.524 ± 0.001) m, generating an FLM spectrum with a FSR of 12 nm. To generate the first harmonic of the Vernier effect (see Fig. 4), the length of the IEC fiber was (1.041 ± 0.001) m. During the strain characterization, the two Hi-Bi fibers were simultaneously stretched. To obtain the enhanced case of the Vernier effect, each fiber presents opposite strain sensitivity, i.e., the IEC fiber has a positive sensitivity and e-core has a negative sensitivity [23].

IV. Results

The Vernier spectrum contains two components, the carrier and the envelope. When the two-fiber loop mirrors have similar optical path lengths, the fundamental Vernier effect is generated. Fig. 3a contains the initial output spectrum and Fig. 3b represents the spectral shift when strain is applied. For the carrier a sensitivity of (13.3 ± 0.3) pm/με with an r^2 of 0.990 was obtained, as seen in Fig. 5. The value corresponds to the algebraic sum between the sensitivities of each Hi-Bi fiber section. In addition, the FSR is 10 nm. A linear strain sensitivity of (80.0 ± 0.3) pm/με with an r^2 of 0.9994 was obtained for the Vernier envelope (Fig. 5), which results in an *M*-factor of 5. Moreover, the FSR is 40 nm. The structure presents then an M_{FSR}-factor of 4 and M_{Sens}-factor is 6. Thus, M_{Vernier} is 1.5. When the FSR of one of the fiber loop mirrors is close to twice the FSR of the other fiber loop mirror, the first harmonic of the Vernier effect is introduced. Fig. 4a contains the initial output spectrum for the first harmonic and Fig. 4b represents the spectral shift when strain is applied. The relationship between the applied strain and the wavelength shift of the Vernier envelope is also depicted in Fig. 5. A linear strain sensitivity of (120 ± 1) pm/με with r^2 of 0.9990 was obtained for the envelope, which implies an *M*-factor of 8. Furthermore, the envelope FSR is 30 nm and the carrier FSR is 5 nm. Hence, the first harmonic structure presents an M_{FSR}-factor of 6 and M_{Sens}-factor is 9. Thus, M_{Vernier} is 1.5. These Hi-Bi fibers were also implemented in single fiber loop mirrors and their strain response is well characterized and published in the literature [23]. Nevertheless, both fibers were here independently characterized. For the IEC fiber section, a sensitivity of (15.46 ± 0.02) pm/με with an r^2 of 0.99993 was determined. For the e-core fiber section, a sensitivity of (-2.41 ± 0.01) pm/με with an r^2 of 0.9998 was obtained (Fig. 5).

V. Conclusion

This research demonstrates a strain sensor that provides higher sensitivity than traditional FLM sensors. The enhanced Vernier effect was here applied by using two FLMs, one with an IEC fiber and the other with an e-core fiber, with opposite sensitivity values. Independently, the FLM with an IEC fiber achieved a sensitivity of (15.46 ± 0.02) pm/με, while the FLM with an e-core reached a sensitivity of (-2.41 ± 0.01) pm/με. The work explored fundamental and the first harmonic of the Vernier effect by combining the two FLMs in a parallel configuration. In the Vernier spectrum, a sensitivity of (13.3 ± 0.3) pm/με was obtained for the carrier. The Vernier envelope achieved a sensitivity of (80.0 ± 0.3) pm/με, with an *M*-factor of 5, for the fundamental case. As for the first harmonic of the Vernier effect, the envelope reached a sensitivity of (120 ± 1) pm/με, with an *M*-factor of 8. For both cases the M_{Vernier} is 1.5 (eq. 8). Considering that the minimum resolution of OSA is 0.02 nm, the minimum measurement step is 0.2 με.

Furthermore, increasing the length of the Hi-Bi optical fiber to introduce optical harmonics of the Vernier effect, increases spectral frequency of the carrier. This makes it easier to trace and track the internal Vernier envelopes, favoring their analysis. Therefore, this sensor has great capacity for applications in large structures such as bridges, buildings, tunnels, and pipelines, or as a displacement sensor.

References

[1] R. J. Potter, "Transmission Properties of Optical Fibers", *OSA*, vol. 51, iss. 10, pp. 1079-1089, 1961, DOI: 10.1364/JOSA.51.001079.

[2] M. Nakazawa, E. Yamada, H. Kubota, K. Suzuki, "10 Gbit/s soliton data transmission over one million kilometres", *IET*, vol. 27, iss. 14, pp. 1270-1272, July 1991, DOI: 10.1049/el:19910796.

[3] M. P. Varnham, A. J. Barlow, D. N. Payne, K. Okamot, "Polarimetric strain gauges using high birefringence fibre", *IET*, vol. 19, iss. 17, Aug. 1983, DOI: 10.1049/el:19830476.

[4] J. Liang, Qi Mo, S. Fu, M. Tang, P. Shum, D. Liu, "Design and fabrication of elliptical-core few-mode fiber for MIMO-less data transmission", *Optics Letters*, vol. 41, iss. 13, pp. 3058 – 3061, June 2016, DOI: 10.1364/OL.41.003058.

[5] Y.-S. Sun, C.-J. Li, J.-C. Hsu, "Integration of Curved D-Type Optical Fiber Sensor with Microfluidic Chip", *Sensors*, vol. 17, iss. 1, Dec. 2017, DOI: 10.3390/s17010063.

[6] J. Yan, L. Miao, T. Huang, S. Che, X. Shu, "Development of method for polarization alignment of PANDA polarization maintaining fiber", *Optical Fiber Technology*, vol. 53, p. 101999, Aug. 2019, DOI: 10.1016/j.yofte.2019.101999.

[7] S. Chen, J. Wang, "Fully degeneracy-lifted bow-tie elliptical ring-core multi-mode fiber", *Optics Express*, vol. 26, iss. 14, pp. 18773 – 18782, Jul. 2018, DOI: 10.1364/OE.26.018773.

[8] I Abe, V de Oliveira, R Fiorin, H J Kalinowski, "Thermal characterization of Bragg gratings in polarization-maintaining optical fibres: analysis of birefringence and regeneration", *Meas. Sci. Technol.*, vol. 28, p. 045206, Feb. 2017, DOI: 10.1088/1361-6501/aa5d4a.

[9] X.-G. Li, Y. Zhao, Lu Cai, X. Zhou, "Measurement of Magnetic Field and Temperature Based on Fiber-Optic Composite Interferometer", *IEEE Transactions on Instrumentation and Measurement*, vol. 66, no. 7, pp. 1906 – 1911, July 2017, DOI: 10.1109/TIM.2017.2670067.

[10] P. Zua, C. C. Chanb, P. L. So, "Sensitivity dependence of fiber loop mirror on the length of high birefringence fiber", *Sensors and Actuators A: Physical*, vol. 247, pp. 393 – 396, Aug. 2016, DOI: 10.1016/j.sna.2016.06.023.

[11] P. Zu, P. L. So, C. C. Chan, "An Ultrahigh Sensitivity Point Temperature Sensor Based on Fiber Loop Mirror", *IEEE Journal of Selected Topics in Quantum Electronics*, vol. 23, iss. 2, no. 5601204, April 2017, DOI: 10.1109/JSTQE.2016.2627181.

[12] W. Qian, C. Zhao, X. Dong, W. Jin, "Intensity measurement based temperature-independent strain sensor using a highly birefringent photonic crystal fiber loop mirror", *Optics Communications*, vol. 283, iss. 24, pp. 5250 – 5254, Dec. 2010, DOI: 10.1016/j.optcom.2010.07.062.

[13] H. Y. Fu, H. Y. Tam, L. Shao, X. Dong, P. K. A. Wai, C. Lu, S. K. Khijwania, "Pressure sensor realized with polarization-maintaining photonic crystal fiber-based Sagnac interferometer", *Applied Optics*, vol. 47, iss. 15, pp. 2835 – 2839, May 2008, DOI: 10.1364/AO.47.002835.

[14] X. Wanga, S. Lou, X. Sheng, S. Liang, "Simultaneous measurement of torsion, strain and temperature using a side-leakage photonic crystal fiber loop mirror", *Infrared Physics & Technology*, vol. 76, pp. 603 – 607, May 2016, DOI: 10.1016/j.infrared.2016.04.029.

[15] X. Zhang, L. Ren, X. Wu, H. Li, L. Liu, L. Xu, "Coupled optofluidic ring laser for ultrahigh- sensitive sensing", *Optics Express*, vol. 19, iss. 22, pp. 22242 – 22247, Oct. 2011, DOI: 10.1364/OE.19.022242.

[16] Z. Xu, Q. Sun, B. Li, Y. Luo, W. Lu, D. Liu, P. P. Shum, L. Zhang, "Highly sensitive refractive index sensor based on cascaded microfiber knots with Vernier effect", *Optics Express*, vol. 23, iss. 5, pp. 6662 – 6672, Mar. 2015, DOI: 10.1364/OE.23.006662.

[17] A. D. Gomes, M. S. Ferreira, J. Bierlich, J. Kobelke, M. Rothhardt, H. Bartelt, O. Frazão, "Optical Harmonic Vernier Effect: A New Tool for High Performance Interferometric Fibre Sensors", *Sensors*, vol. 19, iss. 24, Dec. 2019, DOI: 10.3390/s19245431.

[18] J. Deng, D. N. Wang, "Ultra-sensitive Strain Sensor Based on Femtosecond Laser Inscribed In-fiber Reflection Mirrors and Vernier Effect", *Journal of Lightwave Technology*, vol. 37, no. 19, pp. 4935-4939, Oct. 2019, DOI: 10.1109/JLT.2019.2926066.

[19] A. D. Gomes, M. S. Ferreira, J. Bierlicha, J. Kobelkea, M. Rothhardta, "Hollow microsphere combined with optical harmonic Vernier effect for strain and temperature discrimination", *Optics & Laser Technology*, vol. 127, p. 106198, Feb. 2020, DOI: 10.1016/j.optlastec.2020.106198.

[20] L. Liu, T. Ning, J. Zheng, Li Pei, J. Li, J. Cao, X. Gao, C. Zhang, "High-sensitivity strain sensor implemented by hybrid cascaded interferometers and the Vernier-effect", *Optics & Laser Technology*, vol. 119, p. 105591, May 2019, DOI: 10.1016/j.optlastec.2019.105591.

[21] S. Liu, P. Lu, E. Chen, W. Ni, D. Liu, J. Zhang, Z. Lian, "Vernier effect of fiber interferometer based on cascaded PANDA polarization maintaining fiber", *Chinese Optics Letters*, vol. 17, iss. 8, no. 08601, Aug. 2019, DOI: 10.3788/COL201917.080601.

[22] D. Leandro, A. L.-Aldaba, M. Bravo, M. L.-Amo, Monitoring Multiple Hi-Bi Sensing Fibers in a Single Fiber Loop Mirror", *Journal of Lightwave Technology*, vol. 34, no. 19, pp. 4543 – 4549, Oct. 2016, DOI: 10.1109/JLT.2016.2523880.

[23] O. Frazão, J. M. Baptista, J. L. Santos, "Recent Advances in High-Birefringence Fiber Loop Mirror Sensors", *Sensors*, vol. 7, iss. 11, pp. 2970 – 2983, Nov. 2007, DOI: 10.3390/s7112970

[24] J. Li, M. Zhang, M. Wan, C. Lin, S. Huang, C. Liu, Q. He, X. Qiu, X. Fang, "Ultrasensitive refractive index sensor based on enhanced Vernier effect through cascaded fiber core-offset pairs", *Optics Express*, vol. 28, iss. 3, pp. 4145 – 4155, Feb. 2020, DOI: 10.1364/OE.384815.

[25] S. Zhang, Y. Liu, H. Guo, Ai Zhou, Libo Yuan, "Highly Sensitive Vector Curvature Sensor Based on Two Juxtaposed Fiber Michelson Interferometers With Vernier-Like Effect", *IEEE Sensors Journal*, vol. 19, no. 6, pp. 2148-2154, Mar. 2019, DOI: 10.1109/JSEN.2018.2884889.